Computational Materials Science 139 (2017) 225–233

Contents lists available at ScienceDirect

Computational Materials Science

journal homepage: www.elsevier.com/locate/commatsci

Development and application of Ni-Ti and Ni-Al-Ti 2NN-MEAM interatomic potentials for Ni-base superalloys

Young-Kwang Kim [a], Hong-Kyu Kim [b], Woo-Sang Jung [c], Byeong-Joo Lee [a,*]

[a] Department of Materials Science and Engineering, Pohang University of Science and Technology (POSTECH), Pohang 790-784, Republic of Korea
[b] Energetics and Defense Materials R&D Institute, Agency for Defense Development (ADD), Daejeon 305-600, Republic of Korea
[c] High Temperature Energy Materials Research Center, Korea Institute of Science and Technology, Seoul 136-791, Republic of Korea

ARTICLE INFO

Article history:
Received 19 May 2017
Received in revised form 2 August 2017
Accepted 3 August 2017
Available online 12 August 2017

Keywords:
Atomistic simulation
Ni-Al-Ti superalloys
Modified embedded-atom method

ABSTRACT

Interatomic potentials for the Ni-Ti and Ni-Al-Ti systems have been developed based on the second nearest-neighbor modified embedded-atom method (2NN-MEAM) formalism. The Ni-Ti binary potential reproduces fundamental materials properties (structural, elastic, thermodynamic, and thermal stability) of alloy systems in reasonable agreement with experiments, first-principles calculations and thermodynamic calculations. Atomistic simulations using the Ni-Al-Ti ternary potential validate that the potential can be applied successfully to atomic-scale investigations to clarify the effects of titanium on important materials phenomena (site preference in γ′, γ-γ′ phase transition, and segregation on grain boundaries) in Ni-Al-Ti ternary superalloys.

1. Introduction

Titanium is one of the major alloying elements for Ni-base superalloys. High-temperature mechanical properties of Ni-base superalloys are affected by alloying Ti through various microstructural factors such as dislocations, diffusion, grain boundaries, twinning, stacking faults, partitioning between the γ and γ′ phases, precipitates, and site preference in γ′ [1–3]. To deal with the addition of Ti, it is necessary to know how Ti will affect the microstructural factors more clearly and quantitatively. Since those microstructural factors have an origin in atomic-scale materials phenomena, it is generally difficult to interpret them experimentally. In this case, one can use first-principles calculations or (semi-)empirical atomic simulations as an alternative. First-principles studies have revealed the effects of Ti on antiphase boundary energy [4], elastic properties [5,6], and stacking fault energy [4,7]. Because of the limitation in the sample size that can be handled using first-principles calculations [8], atomistic simulations using (semi-)empirical interatomic potentials are necessary to study more practical materials phenomena such as fracture, diffusion, segregation, and dislocation slip. In this case, the reliability of the interatomic potential has a critical effect on the validity of simulations.

A minimum requirement for the atomic-scale study of Ti effect on materials properties of Ni-base superalloys mostly applied in engineering fields may be the interatomic potential for the Ni-Al-Ti ternary system. The interatomic potential used for this purpose should be the one that can handle all the constituent elements simultaneously based on a single formalism. In addition, the potential should reproduce correctly the site preference of Ti in the γ′ phases and γ-γ′ equilibrium phase boundaries. Until now, there is only one published interatomic potential for the Ni-Al-Ti ternary system, the embedded atom method (EAM) potential by Farkas et al. [9]. The EAM potential can reproduce the fundamental materials (structural, elastic, and thermodynamic) properties of intermetallic compounds related to martensitic transformation for binary and ternary systems [9]. However, its performance for the site preference of Ti in the γ′ phases and the γ-γ′ equilibrium phase boundaries is not known. Baskes proposed modified embedded atom method (MEAM) interatomic potential that can cover various elements simultaneously [10]. Removing some critical flaws in the MEAM, Lee and Baskes modified it to take into account the second nearest-neighbor interaction. This modified potential is called the second nearest-neighbor modified embedded atom method (2NN-MEAM) interatomic potential; it has been applied to various multi-component systems [11–14].

To complete a Ni-Al-Ti ternary potential, one needs potentials for pure elements and the three (Ni-Al, Al-Ti and Ni-Ti) binary systems. 2NN-MEAM interatomic potentials for Ni [13], Al [13], and Ti [15], and those for Ni-Al [16] and Al-Ti [17] binary systems were

* Corresponding author.
E-mail address: calphad@postech.ac.kr (B.-J. Lee).

http://dx.doi.org/10.1016/j.commatsci.2017.08.002
0927-0256/

already available from the work of the present authors' group. Recently, Ko et al. [18] also published a 2NN-MEAM interatomic potential for the Ni-Ti binary system. This potential can reproduce not only the martensitic transformation between B19′ and B2 structures but also the properties of other phases. However, this potential could not be used in the present study to complete the Ni-Al-Ti ternary potential by combining with the already developed Ni-Al and Al-Ti binary potentials. This was because the potential parameters for pure Ni and Ti proposed by Ko et al. [18] were different from those for the Ni [13] and Ti [15] unary potentials used to develop the Ni-Al [16] and Al-Ti [17] binary potentials. Therefore, the 2NN-MEAM interatomic potential for the Ni-Ti binary system needed to be developed again to obtain a description for the ternary system. An ideal interatomic potential for a binary system should reproduce the fundamental materials (structural, elastic, thermodynamic, and thermal) properties of solutions and intermetallic compounds on the phase diagram. There have been several interatomic potentials developed for the Ni-Ti binary system beyond the 2NN-MEAM by Ko et al. [18]: an F-S (Finnis-Sinclair) by Lai and Liu [19], MEAM by Ishida and Hiwatari [20] and Saitoh et al. [21], and modified F-S by Mutter and Nielaba [22] and Zhong et al. [23]. These are potentials developed mainly to reproduce the martensitic transformation between B19′ and B2 structures. It is not well documented how they reproduce the properties of other phases.

The objective of this work is to develop a 2NN-MEAM interatomic potential for the Ni-Al-Ti ternary system. With the already available Ni-Al [16] and Al-Ti [17] potentials, the main task is to develop the Ni-Ti binary potential based on the Ni [13] and Ti [15] potentials used to develop the other binary potentials [16,17], and to extend it to the Ni-Al-Ti ternary system. We briefly describe potential parameters and parameterization procedures for the Ni-Ti binary and the Ni-Al-Ti ternary systems in Section 2, examine the reliability and transferability of the potentials in Section 3, and conclude in Section 4.

2. Interatomic potential

As mentioned earlier, the 2NN-MEAM potentials for pure Ni [13], Al [13], Ti [15] and Ni-Al [16], Al-Ti [17] binary systems have been already published, and the parameter sets are presented in Tables 1 and 2.

For a unary potential, there are 14 independent parameters. The cohesive energy (E_c), equilibrium nearest-neighbor distance (r_e), bulk modulus (B) of the reference structure and an adjustable parameter (d) are model parameters for the universal equation of state. The other model parameters ($\beta^{(0)}$, $\beta^{(1)}$, $\beta^{(2)}$, $\beta^{(3)}$, $t^{(1)}$, $t^{(2)}$, $t^{(3)}$, A, $C_{\min}$, $C_{\max}$) are for electron density, embedding function and many-body screening. Details of the 2NN-MEAM formalism are available in the Refs. [11–14], and are also provided as a supplementary material.

2.1. Parameterization for the Ni-Ti binary system

For a binary potential, there are 13 independent parameters: four (E_c, r_e, B, and d) for the universal equation of state for the reference structure, one (ρ_0) for the electron density ratio, and eight (four $C_{\min}$ and four $C_{\max}$) for many-body screening. Fundamental alloy properties from experiments, first-principles calculations and thermodynamic calculations are used to optimize the parameter values.

To optimize the values of E_c, r_e, and B, a reference structure should first be defined. The reference structure for a binary system is a simple compound structure in which one type of atoms has only the same type of atoms as its second nearest-neighbors. If a stable compound is chosen as the reference structure, the E_c, r_e, and B values can be determined from the experimental information. There are four stable compounds in the Ni-Ti binary phase diagram [24]: $D0_{24}$ Ni_3Ti, B19′ NiTi, B2 NiTi, and $E9_3$ $NiTi_2$. The B2 NiTi compound has the simplest structure and meets the crite-

Table 1
2 NN-MEAM potential parameters for individual elements. The units of E_c, r_e, and B are eV, Å, and 10^{12} dyne/cm^2, respectively. The reference structures are fcc Ni, fcc Al, and hcp Ti.

Ele.	E_c	r_e	B	A	$\beta^{(0)}$	$\beta^{(1)}$	$\beta^{(2)}$	$\beta^{(3)}$	$t^{(1)}$	$t^{(2)}$	$t^{(3)}$	C_{min}	C_{max}	d
Ni[a]	4.45	2.49	1.876	0.94	2.56	1.50	6.00	1.50	3.10	1.80	4.36	0.81	2.80	0.05
Al[a]	3.36	2.86	0.794	1.16	3.20	2.60	6.00	2.60	3.05	0.51	7.75	0.49	2.80	0.05
Ti[b]	4.87	2.92	1.100	0.66	2.70	1.00	3.00	1.00	6.80	−2.00	−12.00	1.00	1.44	0.00

[a] Ref. [13].
[b] Ref. [15].

Table 2
2NN-MEAM potential parameters for individual binary systems. The units of E_c, r_e, and B are eV, Å, and 10^{12} dyne/cm^2, respectively.

	Ni-Al [16]	Al-Ti [17]	Ni-Ti
Reference structure	BCC_B2	BCC_B2	BCC_B2
E_c	4.53	4.375	5.012
r_e	2.4916	2.8	2.57
B	1.58	1.426	1.420
C_{min}(A-B-A)	1.6	$0.49(C_{\min}^{Al})$	0.68
C_{min}(B-A-B)	$0.49(C_{\min}^{Al})$	1.3	0.36
C_{min}(A-A-B)	$0.64([0.5(C_{\min}^{Ni})^{1/2} + 0.5(C_{\min}^{Al})^{1/2}]^2)$	$0.72([0.5(C_{\min}^{Al})^{1/2} + 0.5(C_{\min}^{Ti})^{1/2}]^2)$	0.44
C_{min}(A-B-B)	$0.64([0.5(C_{\min}^{Ni})^{1/2} + 0.5(C_{\min}^{Al})^{1/2}]^2)$	0.46	0.23
C_{max}(A-B-A)	$2.8(C_{\max}^{Ni})$	1.44	1.44
C_{max}(B-A-B)	$2.8(C_{\max}^{Al})$	2.8	1.44
C_{max}(A-A-B)	1.44	2.8	1.44
C_{max}(A-B-B)	$2.8([0.5(C_{\max}^{Ni})^{1/2} + 0.5(C_{\max}^{Al})^{1/2}]^2)$	1.44	1.44
d	$0.5d^{Ni} + 0.5\ d^{Al}$	$0.5\ d^{Al} + 0.5d^{Ti}$	$0.5d^{Ni} + 0.5d^{Ti}$
ρ_0	$\rho_0^{Ni} = \rho_0^{Al} = 1$	$\rho_0^{Al} = \rho_0^{Ti} = 1$	$\rho_0^{Ni} = \rho_0^{Ti} = 1$

rion of the reference structure, and therefore, is chosen as the reference structure.

The values of E_c and B are determined from experimental information on the heat of formation [25] and the bulk modulus [26] of the B2 NiTi compound, respectively. For better quality of the potential, the value r_e is determined from experimental information on the lattice constants of the fcc Ni-Ti alloys [27-31] as well as those of the B2 NiTi compound. With a lack of necessary information, an average of unary values is given to the parameter d. Similarly, the atomic electron density ratio between Ni and Ti is assumed to be equal to one. All the C_{min} and C_{max} values are optimized to maintain structural stability of the B19′ and B2 NiTi compounds at finite temperatures. Table 2 shows the finally optimized potential parameter set.

2.2. Parameterization for the Ni-Al-Ti ternary system

In addition to constituent unary and binary parameters, six more parameters (three C_{min} (i-k-j) and three C_{max} (i-k-j)) need to be defined further to describe a ternary system. The C_{min} (i-k-j) and C_{max} (i-k-j) represent the degree of screening by a third element atom (k) to the interaction between two neighboring atoms (i and j) of different types. We have estimated these parameter values based on a kind of averaging concept between binary C_{min} and C_{max} values [16,32,33] due to the difficulty in finding necessary information to uniquely determine the values. Ti is generally known to prefer the Al site in the γ′ Ni_3Al phase [6,34,35], which is not sufficient to uniquely determine the ternary parameters. When mechanically estimating the ternary C parameters, we assumed that Ni and Al have characters similar to each other compared to Ti. Among the probable ternary parameter sets, we choose the one that best reproduces the site preference of Ti in the $L1_2$ Ni_3Al structure. Table 3 presents the finally chosen ternary parameters.

3. Calculation of materials properties

In this section, we evaluate the reliability of the developed potentials by comparing the calculated materials properties with available information from experiments and/or other calculations. The 2NN-MEAM formalism includes up to second nearest-neighbor interactions, and the radial cutoff distance during atomistic simulations should be at least larger than the second nearest-neighbor distance in the structures under consideration. The radial cutoff distance used in all calculations is 5.0 Å which is larger than the second nearest-neighbor distance of pure Ti, the element with the largest nearest distance among the elements considered. If not designated, all calculations are performed at 0 K, using an in-house code, KISSMD [14,36].

The Ni-Ti binary phase diagram [24] consists of liquid, fcc, hcp, and bcc solid solutions, as well as $D0_{24}$ Ni_3Ti, B19′ NiTi, B2 NiTi, and $E9_3$ $NiTi_2$ compounds. The NiTi compounds have a martensitic transition between the B19′ and B2 structures; this is the main materials phenomenon of Ni-Ti shape memory alloys. Here, the B19′ NiTi phase is the stable phase below room temperature, and the B2 NiTi phase is the stable phase above room temperature [24]. The potential parameters for the Ni-Ti binary system were optimized using the experimental information on lattice constants of the fcc Ni-Ti solid solution, the heat of formation and the bulk modulus of B2 NiTi, and the structural stability of B2 and B19′ NiTi. The experimental information on heat of formation, bulk modulus and lattice constants of other stable intermetallic compounds, heat of mixing of liquid, and structural stability of stable phases was used for the evaluation of the transferability of the potential.

Table 3
2 NN-MEAM potential parameters (C_{max} and C_{min}) for the Ni-Al-Ti ternary system.

Type		Parameter	Assumption
C_{max}	(Ni-Ti-Al)	1.44	$[0.5(C^{Ni\text{-}Ti\text{-}Ni})^{1/2} + 0.5(C^{Al\text{-}Ti\text{-}Al})^{1/2}]^2$
	(Ni-Al-Ti)	1.44	$C^{Ni\text{-}Ni\text{-}Ti}$
	(Al-Ni-Ti)	2.80	$C^{Al\text{-}Al\text{-}Ti}$
C_{min}	(Ni-Ti-Al)	0.58	$[0.5(C^{Ni\text{-}Ti\text{-}Ni})^{1/2} + 0.5(C^{Al\text{-}Ti\text{-}Al})^{1/2}]^2$
	(Ni-Al-Ti)	0.44	$C^{Ni\text{-}Ni\text{-}Ti}$
	(Al-Ni-Ti)	0.72	$C^{Al\text{-}Al\text{-}Ti}$

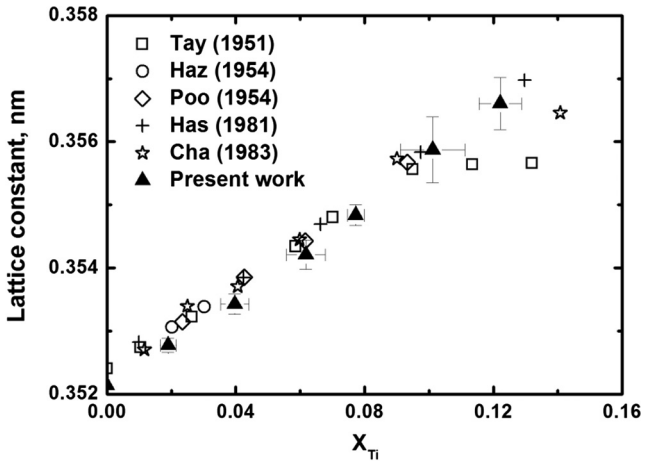

Fig. 1. Comparison between calculated lattice constant of fcc Ni-xTi alloys (0 K) and literature data (298 K) [27–31].

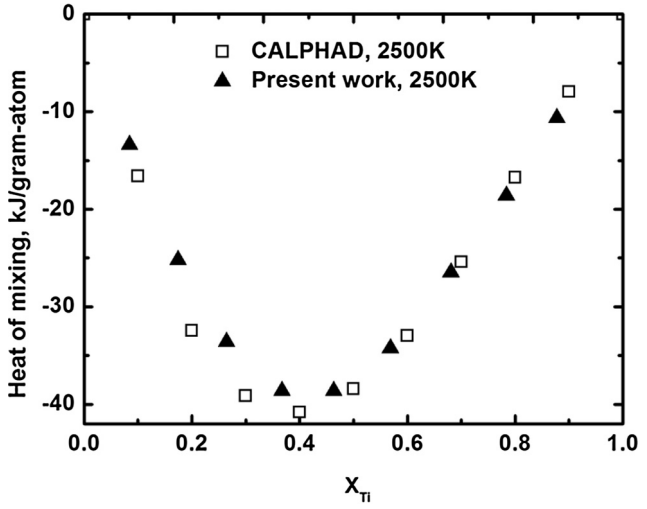

Fig. 2. Comparison between calculated heat of mixing of liquid Ni-xTi alloys and a CALPHAD calculation [37].

Fig. 1 shows the lattice constant of the fcc Ni-Ti solid solution according to the present potential, in comparison with experiments [27–31]. Each value is an average of ten calculations with cubic samples (864 atoms) of random, disordered solid solution. Fig. 2 compares the calculated heat of mixing of liquid with a CALPHAD calculation. A molecular dynamics (MD) with a Nose-Hoover thermostat, a Parrinello-Rahman NPT ensemble and a velocity Verlet algorithm is used for this calculation. Initial samples with 2048 atoms were heated to 2500 K. The enthalpy of each sample was calculated at 2500 K during 50,000 steps (1 time step = 2 fs) for equilibration, averaged for the last 20,000 steps. Table 4 compares the calculated fundamental materials properties (heat of formation, bulk modulus, lattice constants, and monoclinic angle) of four

Table 4
Calculated materials properties of Ni_3Ti, NiTi, and $NiTi_2$ compounds in comparison with experimental information and other calculations. Values listed are lattice constants, *a*, *b*, *c* (nm), monoclinic angle β (degree), atomic volume Ω ($Å^3$), bulk modulus *B* (GPa), and heat of formation ΔH_f (eV/atom).

Structure	Property	Exp.	Present work	FP calc. [18]	2NN-MEAM [18]
$D0_{24}$ Ni_3Ti	*a*	0.5101,[a] 0.5109[b]	0.508	0.5108	0.5158
	c	0.8307,[a] 0.8319[b]	0.833	0.8337	0.835
	B	163.4[c]	166.9	190.6	154.5
	ΔH_f	−0.36[d]	−0.330	−0.487	−0.349
B2 NiTi	*a*	0.3016[e]	0.2968	0.3012	0.2999
	b	0.4265[e]	0.4197	0.426	0.4242
	c	0.4265[e]	0.4197	0.426	0.4242
	β	90[e]	90	90	90
	Ω		13.07	13.67	13.49
	B	142[f]	142	157.1	133.2
	ΔH_f	−0.353,[g] −0.351[d]	−0.351	−0.355	−0.393
B19′ NiTi	*a*	0.2884,[h] 0.2909[e]	0.2783	0.2945	0.2878
	b	0.4110[h], 0.4114[e]	0.4183	0.4034	0.4129
	c	0.4657,[e] 0.4665[h]	0.4533	0.4769	0.4659
	β	97.9,[e] 98.1[h]	98.4	101.8	99.4
	Ω		13.19	13.87	13.66
	B		141	158	134
	$E\text{-}E_{B2}$		−0.0091	−0.0428	−0.0341
$E9_3$ $NiTi_2$	*a*	1.128,[i] 1.132[b]	1.1204	1.128	1.13
	B		126.3	143.7	119.8
	ΔH_f	−0.278[d]	−0.265	−0.28	−0.293

[a] Ref. [38].
[b] Ref. [29].
[c] Ref. [39].
[d] Ref. [25].
[e] Ref. [40].
[f] Ref. [26].
[g] Ref. [37].
[h] Ref. [41].
[i] Ref. [42].

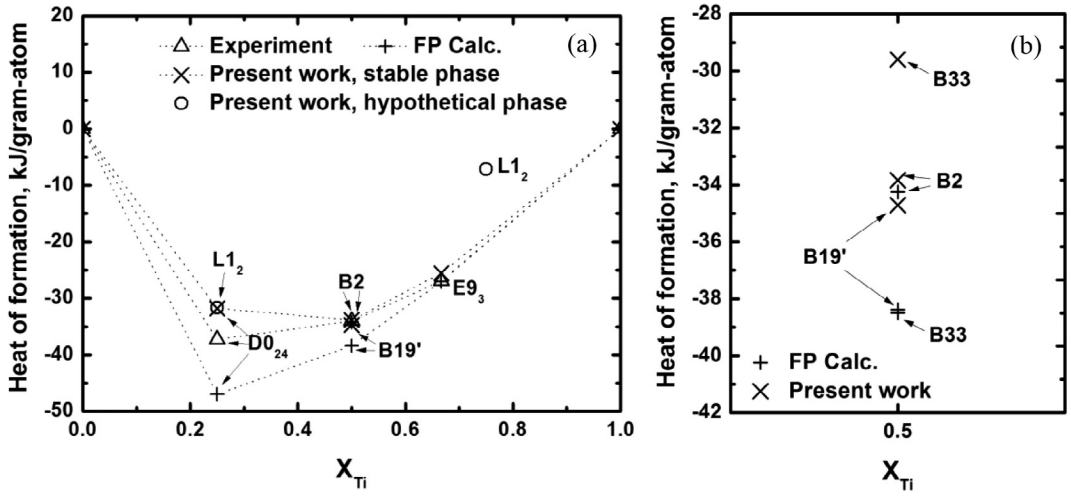

Fig. 3. (a) Comparison between calculated heat of formation for stable or hypothetical intermetallic compounds and literature data [18,25], and (b) comparison between the present calculation for NiTi compounds and a first-principles calculation [18].

stable intermetallic compounds with relevant experimental information, first-principles calculations, and other empirical calculations.

To confirm that the present potential reproduces the stability of stable phases presented in the phase diagram well, we perform two types of calculations. The first is the calculation of the heat of formation of stable and hypothetical intermetallic compounds for each composition. The results are shown in Fig. 3. One can see that the present potential correctly reproduces the most energetically favorable compound for each composition. In the case of NiTi compounds, as shown in Fig. 3(b), the present calculation yields an order of $\Delta H_f^{B19'} < \Delta H_f^{B2} < \Delta H_f^{B33}$, consistent with the experimental observation [24,25], while a first-principles calculation [18] shows a different order in the heat of formation, $\Delta H_f^{B33} < \Delta H_f^{B19'} < \Delta H_f^{B2}$.

The second calculation performed is to confirm the thermal stability of the stable phases at finite temperatures. Initial structure of each phase was heated up to 2400 K using an MD simulation, increasing the temperature by 200 K and equilibrating the structure (of around 2000 atoms) for 30,000 steps (1 time step = 2 fs) at each temperature. Then, the heated structure at each temperature was rapidly cooled to 0 K to confirm that the heated structure

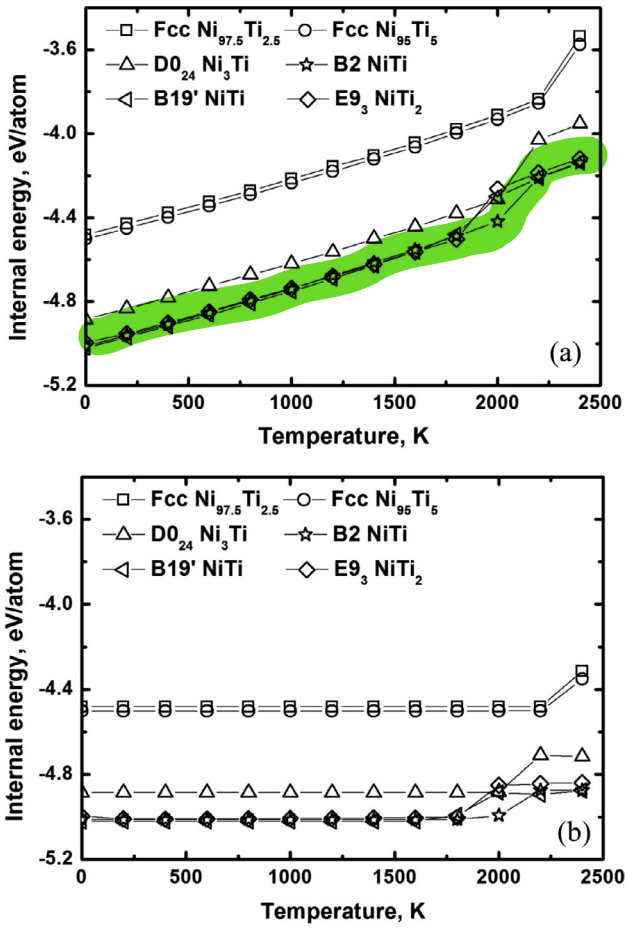

Fig. 4. Change in internal energy of Ni-xTi alloys (a) during heating and (b) after rapid cooling from individual heating temperatures to 0 K.

Table 5
Comparison between calculated specific heat *Cp* (J/mol K) of Ni-Ti alloys at 25 °C and a thermodynamic calculation [37].

Structure	Present work	Calphad [38]
Fcc $Ni_{97.5}Ti_{2.5}$	25.3	26.7
Fcc $Ni_{95}Ti_5$	24.9	27.0
$D0_{24}$ Ni_3Ti	25.8	25.1
B2 NiTi	25.0	29.8
B19′ NiTi	25.4	
$E9_3$ $NiTi_2$	25.0	25.1

is restored to its initial 0 K structure. The objective of this simulation was to see whether the any solid solution or intermetallic compound suffers a phase transformation to a wrong structure, decreasing the energy and thus making itself a stable phase at the corresponding composition. Fig. 4(a) shows the change in internal energy for fcc Ni-Ti solid solutions and intermetallic compounds ($D0_{24}$ Ni_3Ti, B19′ NiTi, B2 NiTi, and $E9_3$ $NiTi_2$) during heating. From these results, it was possible to obtain the specific heat of individual phases, as listed in Table 5. The internal energy of all phases increases monotonically with temperature; the present potential reproduces the specific heat well in comparison with a CALPHAD calculation. Fig. 4(b) presents the internal energy of each crystal structure after rapid cooling to 0 K from each heating temperature. It is confirmed that the original structures are maintained at the heated state. To examine the atomistic structure more clearly, the samples are rapidly cooled to 0 K. When rapidly cooled to 0 K from temperatures below the melting temperature, all the structures except $E9_3$ $NiTi_2$ recover the initial 0 K energy. In the case of the $E9_3$ $NiTi_2$ structure, the rapidly cooled internal energy of $E9_3$ $NiTi_2$ is lower than the initial 0 K energy by −0.013 eV/atom. This is because local relaxations occurred during the rapid cooling simulation but phase transition did not occur.

Unfortunately, the present potential does not reproduce the martensitic transformation between B19′ and B2 structures during the heating and cooling simulation. Ko et al. [18] have already reported that the B19′-B2 phase transition is related to the hcp-bcc phase transition of pure Ti. However, the Ti unary potential [15] used to develop the present potential does not reproduce the hcp-bcc phase transition in pure Ti. This is thought to be the reason why the present potential does not reproduce the B19′-B2 phase transition. One needs to keep this point in mind in future applications of the present potential.

It is revealed that the present binary potential can reproduce fundamental materials properties of Ni-Ti binary alloys reasonably well. One can now extend this binary potential to the Ni-Al-Ti ternary by combining it with the already developed Ni-Al [16] and Al-Ti [17] binary potentials. As mentioned in Section 2.2, the present ternary parameters, shown in Table 3, were determined by considering the experimental information on the site preference of Ti in the γ′ phase. The transferability of the ternary potential could be evaluated through additional simulations. In the present work, simulations for γ-γ′ equilibrium and segregation of Ti on grain boundaries were performed to examine the transferability of the ternary potential.

Table 6 shows the two types of energy mentioned in the literature [16] used to check the site preference of Ti in the γ′ phase. One is the formation energy for the pair of antisite defects (E^{anti}), "$0 \rightarrow Ni_{Al} + Al_{Ni}$". The other is the energy change (exchange energy hereafter) of the reaction corresponding to moving a Ti atom from an Ni site to an Al site in the γ′ phase ($E_{Ti}^{Ni\rightarrow Al}$), "$Ti_{Ni} + Al_{Al} \rightarrow Ti_{Al} + Al_{Ni}$":

$$E_{Ti}^{Ni\rightarrow Al} = E(Ni_{3k}Al_{k-1}Ti) + E(Ni_{3k-1}AlAl_k) - E(Ni_{3k-1}TiAl_k) - E(Ni_{3K}Al_k)$$

where $E(Ni_{3k}Al_{k-1}Ti)$ indicates the energy of the state when a Ti atom replaces an Al atom in the γ′ phase. According to first-principles calculations [6,35], the formation energy for a pair of antisite defects is 1.4–2 eV, while the exchange energy of Ti is −1.0 to −0.62 eV. The present calculation (with 864 atoms) shows that the formation energy for a pair of antisite defects is 2.02 eV, but the exchange energy of Ti is 0.28 eV. As explained in the literature [35], if $E_{Ti}^{Ni\rightarrow Al} < 0$, Ti atoms mostly occupies the Al sites. This is because antisite defects (Al_{Ni}) are easily created. If $E_{Ti}^{Ni\rightarrow Al} > 0$ and the normalized exchange energy, $E = E_{Ti}^{Ni\rightarrow Al}/E^{anti}$, <0.5, a Ti atom weakly prefers an Al site to an Ni site. In this case, it is difficult to estimate quantitatively how many Ti atoms will prefer Al sites.

We additionally performed a Monte Carlo (MC) simulation to investigate the quantitative degree of the Al site preference for the present ternary potential. The MC simulation is based on an isobar-isotherm ensemble (NPT) in which the temperature, the pressure, and the number of particles are maintained constant.

Table 6
Calculated formation energy (E^{anti}) for an antisite pair, "$Ni_{Al} + Al_{Ni}$", and exchange energy ($E_{Ti}^{Ni\rightarrow Al}$) for reaction "$Ti_{Ni} + Al_{Al} \rightarrow Ti_{Al} + Al_{Ni}$" in comparison with literature data [6,35].

	Present work	FP calc.
E^{anti}	2.02	1.40,[a] 2.0[b]
$E_{Ti}^{Ni\rightarrow Al}$	0.28	−0.62,[a] −1.0[b]

[a] Ref. [6].
[b] Ref. [35].

Table 7
Comparison between calculated site fractions in Ni and Al sites of the $L1_2$ structure for the Ni-25at%Al-2at%Ti alloy and a thermodynamic calculation [37].

Element		Calphad [38]	Present work	
			After MC	Before MC
Ni site	Ni	0.973	0.972	0.972
	Al	0.028	0.018	0.000
	Ti	0.000	0.010	0.028
Al site	Ni	0.002	0.000	0.000
	Al	0.918	0.952	1.000
	Ti	0.080	0.048	0.000

The MC simulation considers the vibration of atoms, the exchange of atoms, and the anisotropic change of the sample size, as described in the literature [16]. The system is thought to reach equilibrium when the system energy is no longer reduced. All the Ti atoms initially occupied Ni sites in the initially $L1_2$ Ni-25at%Al-2at%Ti compound. The MC simulation was performed using a cubic sample with 864 atoms at 1173 K for 50,000 steps. The result of the MC simulation is presented in Table 7. According to the present result, the equilibrium site fraction of Ti in the Al sites is smaller than that obtained from a thermodynamic calculation. However, the number of Ti atoms occupying the Al sites is larger than the number of Ti atoms occupying the Ni sites, even though the number of Ni sites is three times larger than the number of Al sites in the $L1_2$ Ni_3Al. One can expect that a Ti atom will prefer an Al sites to an Ni sites in the $L1_2$ Ni_3Al, according to the present potential.

To check the transferability of the ternary potential, first, we examined the γ-γ′ two-phase equilibrium. For this, we performed a grand canonical Monte Carlo (GCMC) simulation. A GCMC simulation for a binary system generates an equilibrium composition, atomic configuration, and volume for a given chemical potential difference between the two elements, $\Delta\mu_{XY}$, and a given temperature. It should be noted here that in a two-phase region of a binary phase diagram the chemical potentials of the two elements and thus the chemical potential difference, $\Delta\mu_{XY}$, are fixed at a given temperature and pressure. If the compositions are calculated as a function of the $\Delta\mu_{XY}$ value, discontinuous change is observed around the $\Delta\mu_{XY}$ value that corresponds to the two-phase equilibrium. The two compositions given by the discontinuous change can be regarded as the boundary compositions of the two-phase equilibrium [43].

The GCMC simulation for a ternary system [44] is based on the methodology mentioned above. It generates volume, atomic configuration, and an equilibrium composition for a given temperature and three types of chemical potential differences, $\Delta\mu_{NiAl}$ (= μ_{Al} − μ_{Ni}), $\Delta\mu_{NiTi}$ (= $\mu_{Ti} - \mu_{Ni}$), and $\Delta\mu_{AlTi}$ (= $\mu_{Ti} - \mu_{Al}$). It should be noted here that one of the three chemical potential differences ($\Delta\mu_{AlTi}$, for example) is determined automatically if the other two differences ($\Delta\mu_{NiAl}$ and $\Delta\mu_{NiTi}$, in this case) are determined uniquely, because there is no change of the total number of atoms in the system. Our GCMC simulation considers changes in atomic positions, sample dimensions in each direction and chemical type of each atom. For example, when a Ni atom is changed to an Al atom, the transition probability (P) is given as

$$P = \left(\frac{m_{Al}}{m_{Ni}}\right)^{\frac{3}{2}} exp\left(\frac{-\Delta\phi}{k_B T}\right),$$

where m_{Ni} and m_{Al} are the atomic masses of Ni and Al, respectively. Here $\Delta\phi$ is

$$\Delta\phi = (E - N_{Al}\mu_{Al} - N_{Ni}\mu_{Ni})_{final} - (E - N_{Al}\mu_{Al} - N_{Ni}\mu_{Ni})_{initial} = E_{final} - E_{initial} - (\mu_{Al} - \mu_{Ni}) = \Delta E - \Delta\mu_{NiAl},$$

where E is the potential energy of the system, N_i the number of atoms of element i, μ_i the chemical potential of element i, ΔE the potential energy difference before and after the MC trial, and $\Delta\mu_{NiAl}$ the chemical potential difference between Ni and Al atoms. Similarly, when an Ni atom is changed to a Ti atom, the transition probability is expressed in terms related to both Ni and Ti atoms. One can obtain equilibrium compositions of Al and Ti from the GCMC simulation by varying the $\Delta\mu_{NiAl}$ value for a given $\Delta\mu_{NiTi}$ value and temperature, observing a discontinuous change around the $\Delta\mu_{NiAl}$ value that corresponds to the γ-γ′ two-phase equilibria. The two compositions given by the discontinuous change corresponds to the compositions of one tie-line in the γ-γ′ two-phase region of the Ni-Al-Ti ternary phase diagram. Using cubic samples with 864 atoms, our GCMC simulations were performed up to 100,000 steps at 1173 K, successively increasing $\Delta\mu_{NiAl}$ with an initially pure fcc Ni sample or successively decreasing $\Delta\mu_{NiAl}$ with an initially $L1_2$ Ni_3Al sample. The last 5000 MC steps were used to collect average values. It was also found through a trial and error that the $\Delta\mu_{NiTi}$ value should be more negative than −1.82 to obtain the γ-γ′ two-phase equilibria using the GCMC simulation at 1173 K.

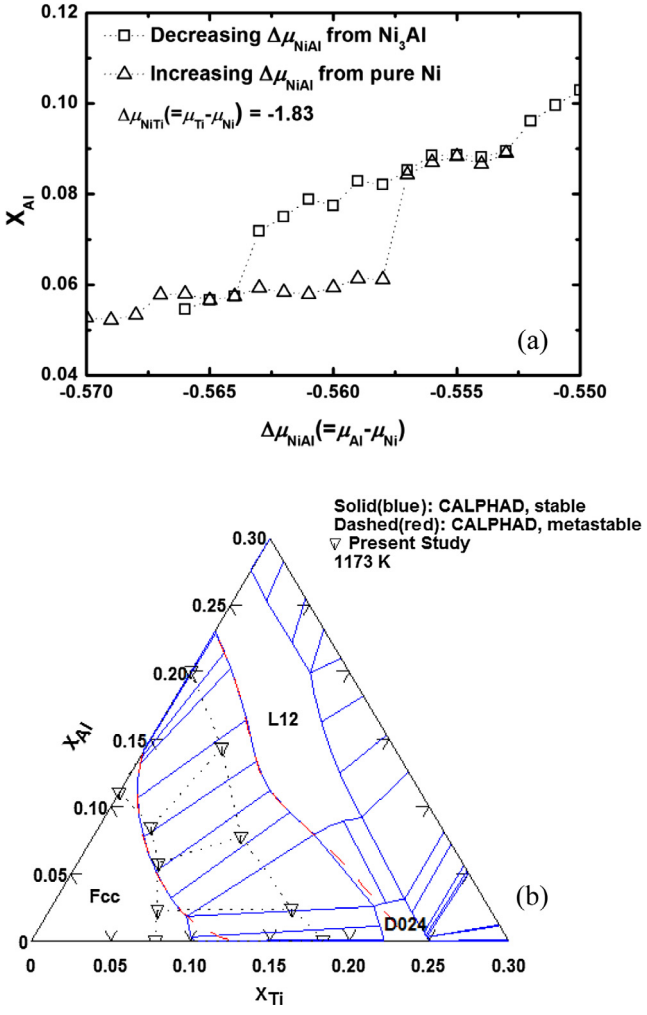

Fig. 5. Calculated γ (Fcc)- γ′ ($L1_2$) two-phase equilibrium for the Ni-Al-Ti ternary system using a grand-canonical Monte Carlo simulation. (a) Mole fraction of Al (x_{Al}) versus $\Delta\mu_{NiAl}$ in the Ni-Al-Ti ternary system for a fixed value of $\Delta\mu_{NiTi}$(=−1.83) at 1173 K and (b) comparison between calculated γ-γ′ equilibrium phase boundaries and a CALPHAD calculation [37]. Equilibrium isothermal section (solid line, blue) and metastable phase boundary between γ (Fcc) and γ′ ($L1_2$) (dashed line, red) are overlapped. (For interpretation of the references to color in this figure legend, the reader is referred to the web version of this article.)

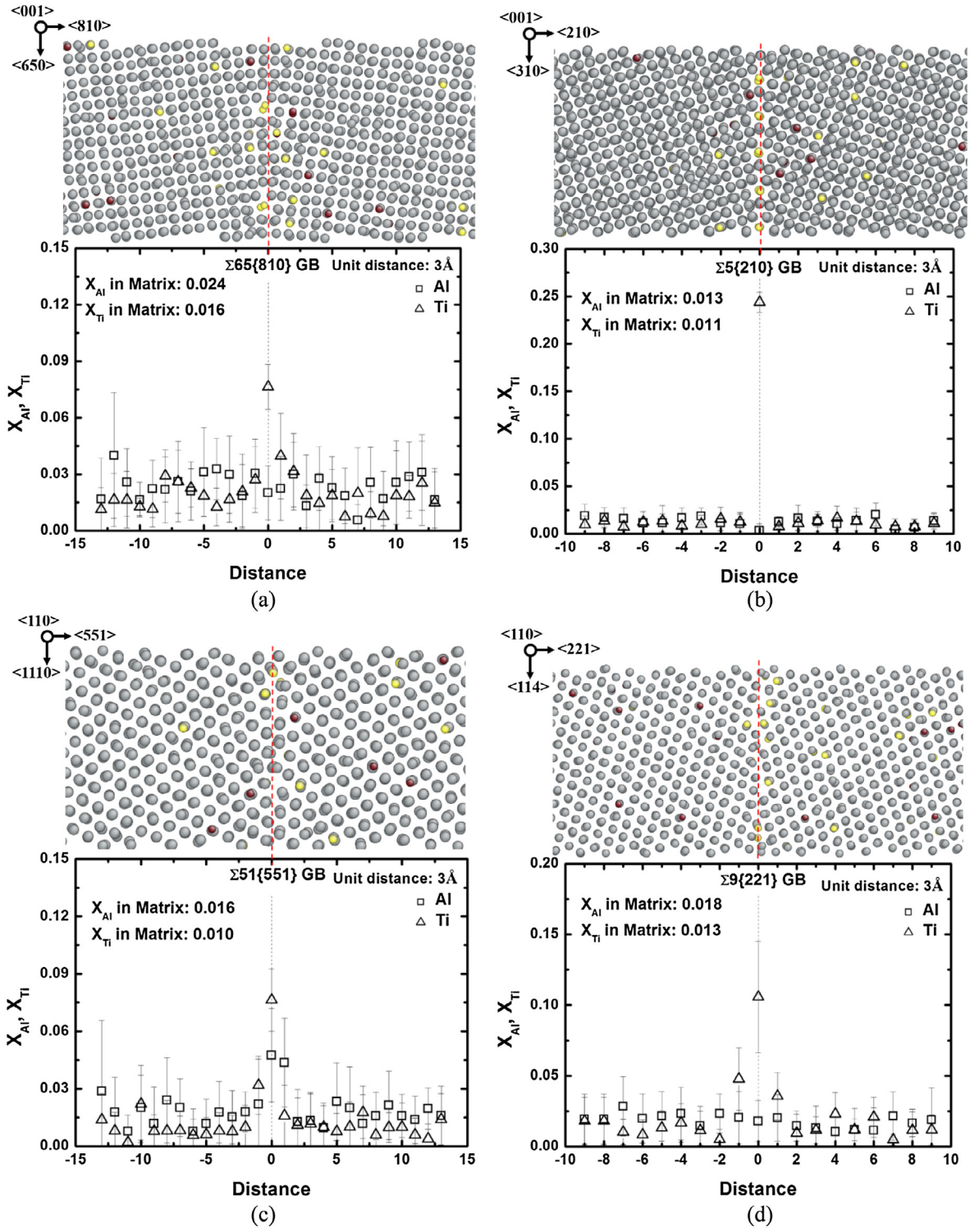

Fig. 6. Mole fractions of Al (x_{Al}) and Ti (x_{Ti}) across (a) Σ65{8 1 0}, (b) Σ5{2 1 0}, (c) Σ51{5 5 1}, and (d) Σ9{2 2 1} tilt grain boundaries in fcc Ni-Al-Ti alloys (γ), by a GCMC simulation for a fixed values of $\Delta\mu_{NiAl}$(=−0.70) and $\Delta\mu_{NiTi}$(=−2.0) at 1173 K after 50,000 MC steps. The red color (dark grey) represents Al atoms, the grey Ni atoms and the yellow (light grey) Ti atoms. (For interpretation of the references to color in this figure legend, the reader is referred to the web version of this article.)

Fig. 5(a) shows the mole fraction of Al (x_{Al}) obtained at 1173 K for a given $\Delta\mu_{NiTi}$ value of −1.83, as a function of the $\Delta\mu_{NiAl}$ value. One can see two curves show a hysteresis. One is what obtained by increasing $\Delta\mu_{NiAl}$ and the other by decreasing $\Delta\mu_{NiAl}$. The hysteresis comes from that it takes a long time to reach equilibrium near the phase boundary inside the two-phase region. Considering the supersaturated compositions in the hysteresis region, the equilibrium phase boundary compositions are selected as the compositions corresponding to the mid-point of the hysteresis. Fig. 5(b) shows the calculated γ-γ′ equilibrium phase boundaries in comparison with the thermodynamic calculations [37] at 1173 K. In Fig. 5(b), three tie-lines are calculated using the ternary GCMC simulation for the given $\Delta\mu_{NiTi}$ values, −1.82, −1.83 and −1.86. Other tie-lines obtained for the Ni-Al and Ni-Ti binary systems are also

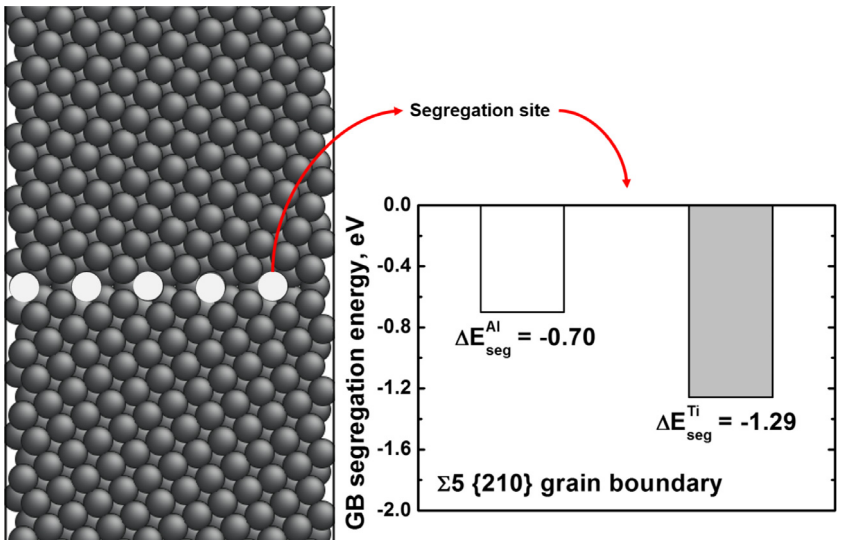

Fig. 7. Calculated segregation energy of Al and Ti on Σ5{2 1 0} tilt grain boundary using the present potential.

presented in this figure. One can see that the present ternary potential reasonably reproduces the γ-γ′ two-phase equilibrium phase boundaries.

The second property examined to evaluate the transferability of the Ni-Al-Ti ternary potential was the segregation of Ti on grain boundaries. It has been experimentally reported that Ti atoms are segregated on grain boundaries [45,46]. The segregation of Ti on grain boundaries was investigated also using the ternary GCMC simulation. Here, the given temperature, $\Delta\mu_{NiAl}$ and $\Delta\mu_{NiTi}$ values are 1173 K, −0.70, and −2.0, respectively, under which condition the bulk composition belongs to the fcc single-phase region, where x_{Al} is 0.016 and x_{Ti} is 0.012. The initial samples were pure fcc Ni samples involving one grain boundary; the grain boundaries considered for this study of the segregation tendency were Σ65{8 1 0} (sample size: 17.4 × 2.9 × 0.8 nm, 3120 atoms), Σ51{5 5 1} (sample size: 21.7 × 2.6 × 0.8 nm, 3672 atoms), Σ5{2 1 0} (sample size: 11.3 × 2.8 × 1.4 nm, 4000 atoms), and Σ9{2 2 1} (sample size: 10.8 × 3.0 × 0.8 nm, 2160 atoms). Ternary GCMC simulations were performed during 50,000 MC steps; the last 3000 steps were used to collect average values. Fig. 6 shows the concentration profiles of Al and Ti plotted around each grain boundary (Σ65{8 1 0}, Σ51{5 5 1}, Σ5{2 1 0}, and Σ9{2 2 1}). The present results show that Ti atoms are more abundant on the grain boundaries than in the matrix, which is in good agreement with the experimental observations [45,46]. In addition, the present calculation shows that the segregation tendency of Al is not prominent in Ni-Al-Ti ternary alloys. On the other hand, there were first-principles studies [47,48] reporting that Al atoms are segregated on the Σ5{2 1 0}grain boundary in Ni-Al binary alloys. Therefore, we examined the segregation tendency of Al and Ti in each Ni-Al and Ni-Ti binary alloy to clarify the difference in Al segregation behavior between binary and ternary alloys.

When a solute atom, X, is present, its segregation energy is calculated as the energy difference between one state in which an X atom is located on a grain boundary site (ΔE^X_{GB}) and another state in which an X atom is located on a matrix site (ΔE^X_{matrix}), yielding the relation:

$$\Delta E^X_{seg} = \min\{\Delta E^X_{GB}\} - \min\{\Delta E^X_{matrix}\},$$

where "min" represent the energetically most stable state. The calculated segregation energy of Al and Ti are −0.70 eV and −1.29 eV, respectively (Fig. 7). The results indicate that the segregation tendency of both atoms is strong, but the segregation tendency of Ti is stronger than that of Al. Therefore, one should understand the non-prominent segregation tendency of Al in Ni-Al-Ti ternary alloys as a result that comes from the much stronger segregation tendency of Ti.

It has been shown that the present ternary potential reproduces site preference of Ti, γ-γ′ phase boundaries, and segregation tendency of Ti on the grain boundaries reasonably well. Therefore, the present potentials for the Ni-Ti binary and Ni-Al-Ti ternary systems can be used to study materials phenomena for Ni-Al-Ti ternary superalloys on an atomic-scale. The most significant advantage of the 2NN-MEAM formalism is that one can easily extend the potentials into higher-order Ni-base superalloy systems by combining the present Ni-Al-Ti potential with already published Ni-Al-Co potential [16], for example.

4. Conclusion

The Ni-Ti binary and Ni-Al-Ti ternary interatomic potentials are now available on the basis of the 2NN-MEAM formalism. The binary potential reproduces the various fundamental materials properties of relevant alloy systems reasonably well. The MD and MC simulations based on the ternary potential show that the ternary potential reproduces the site preference of Ti in γ′, γ-γ′ equilibrium phase boundaries and segregation tendency of Ti on grain boundaries in reasonable agreement with experimental data, first-principles calculations and thermodynamic calculations. Since the important atomic-scale materials phenomena in Ni-base superalloys are correctly reproduced, the present potentials can be further utilized to investigate other atomic-scale materials phenomena such as mechanical properties and thermodynamics behaviors.

Acknowledgements

This work has been financially supported by the Civil Military Technology Cooperation Program (Project No. 13-DU-MP-05) of the Agency for Defense Development-South Korea and the KIST Institutional Programs (Project No. 2E24692).

Appendix A. Supplementary material

Supplementary data associated with this article can be found, in the online version, at http://dx.doi.org/10.1016/j.commatsci.2017.08.002.

References

[1] A.K. Jena, M.C. Chaturvedi, J. Mater. Sci. 19 (1984) 3121.
[2] D. Blavette, E. Cadel, C. Pareige, B. Deconihout, P. Caron, Microsc. Microanal. 13 (2007) 464.
[3] F. Yang, E. Liu, Z. Zhi, J. Tong, L. Ning, Mater. Des. 61 (2014) 41.
[4] X.X. Yu, C.Y. Wang, Mater. Sci. Eng. A 539 (2012) 38.
[5] S.L. Shang, D.E. Kim, C.L. Zacherl, Y. Wang, Y. Du, Z.K. Liu, J. Appl. Phys. 112 (2012) 053515.
[6] Q. Wu, S. Li, Comput. Mater. Sci. 53 (2012) 436.
[7] S.L. Shang, C.L. Zacherl, H.Z. Fang, Y. Wang, Y. Du, Z.K. Liu, J. Phys. Condens. Matter 24 (2012) 505403.
[8] P. Lejcek, M. Sob, V. Paidar, V. Vitek, Scr. Mater. 68 (2013) 547.
[9] D. Farkas, D. Roqueta, A. Vilette, K. Ternes, Modell. Simul. Mater. Sci. Eng. 4 (1996) 359.
[10] M.I. Baskes, Phys. Rev. B 46 (1992) 2727.
[11] B.-J. Lee, M.I. Baskes, Phys. Rev. B 62 (2000) 8564.
[12] B.-J. Lee, M.I. Baskes, H. Kim, Y.K. Cho, Phys. Rev. B 64 (2001) 184102.
[13] B.-J. Lee, J.-H. Shim, M.I. Baskes, Phys. Rev. B 68 (2003) 144112.
[14] B.-J. Lee, W.-S. Ko, H.-K. Kim, E.-H. Kim, Calphad 34 (2010) 510.
[15] Y.-M. Kim, B.-J. Lee, M.I. Baskes, Phys. Rev. B 74 (2006) 014101.
[16] Y.-K. Kim, W.-S. Jung, B.-J. Lee, Model. Simul. Mater. Sci. Eng. 23 (2015) 055004.
[17] Y.-K. Kim, H.-K. Kim, W.-S. Jung, B.-J. Lee, Comput. Mater. Sci. 119 (2016) 1.
[18] W.-S. Ko, B. Grabowski, J. Neugebauer, Phys. Rev. B 92 (2015) 134107.
[19] W.S. Lai, B.X. Liu, J. Phys, Condens. Matter 12 (2000) L53.
[20] H. Ishida, Y. Hiwatari, Mol. Simul. 33 (2007) 459.
[21] K. Saitoh, K. Kubota, T. Sato, Tech. Mech. 30 (2010) 269.
[22] D. Mutter, P. Nielaba, Phys. Rev. B 82 (2010) 224201.
[23] Y. Zhong, K. Gall, T. Zhu, J. Appl. Phys. 110 (2011) 033532.
[24] P. Nash, Phase Diagram of Binary Nickel Alloys, ASM International, 1991.
[25] O. Kubaschewski, H. Villa, W.A. Dench, Trans. Faraday Soc. 52 (1956) 214.
[26] O. Mercier, K.N. Melton, G. Gremaud, J. Häji, J. Appl. Phys. 51 (1980) 1833.
[27] A. Taylor, R.W. Floyd, J. Inst. Met. 80 (1951) 577.
[28] T.H. Hazlett, E.R. Parker, Trans. ASM 46 (1954) 701.
[29] D.M. Poole, W. Hume-Rothery, J. Inst. Met. 83 (1954) 473.
[30] K. Hashimoto, T. Tsujimoto, K. Saito, Trans. Jpn. Inst. Met. 22 (1981) 798.
[31] G. Chattopadhyay, H. Kleykamp, Z. Metallkd. 74 (1983) 182.
[32] H.-K. Kim, W.-S. Jung, B.-J. Lee, Acta Mater. 57 (2009) 3140.
[33] W.-S. Ko, B.-J. Lee, Model. Simul. Mater. Sci. Eng. 21 (2013) 085008.
[34] Y. Mishima, S. Ochiai, T. Suzuki, Acta Metall. 33 (1985) 1161.
[35] A.V. Ruban, H.L. Skriver, Solid State Commun. 99 (1996) 813.
[36] https://cmse.postech.ac.kr/home_2nnmeam.
[37] http://www.thermocalc.com/media/8165/2013-05-31-tcni6_extended_info.pdf.
[38] A. Taylor, R.W. Floyd, Acta Cryst. 3 (1950) 285.
[39] S.V. Prikhodko, D.G. Isaak, J.D. Carnes, S. Moser, Y. Ma, A.J. Ardell, Metall. Mater. Trans. A 34 (2003) 1863.
[40] S.D. Prokoshkin, A.V. Korotitskiy, V. Brailovski, S. Turenne, I.Yu. Khmelevskaya, I.B. Trubitsyna, Acta Mater. 52 (2004) 4479.
[41] W. Buhrer, R. Gotthardt, A. Kulik, O. Mercier, F. Staub, J. Phys. F: Met. Phys. 13 (1983) L77.
[42] G.A. Yurko, J.W. Barton, J.G. Parr, Trans. AIME 212 (1958) 698.
[43] B.-J. Lee, J.-H. Shim, Calphad 28 (2004) 125.
[44] C. Pareige, F. Soisson, G. Martin, D. Blavette, Acta Mater. 47 (1999) 1889.
[45] L. Letellier, S. Chambreland, P. Duval, D. Blavette, Appl. Surf. Sci. 67 (1993) 305.
[46] Y. Pardhi, ed., Metallurgy - Advances in Materials and Processes, Intech, 2012.
[47] M. Yamaguchi, M. Shiga, H. Kaburaki, J. Phys. Condens. Matter 16 (2004) 3933.
[48] M. Všianská, M. Šob, Prog. Mater. Sci. 56 (2011) 817.